Journal Pre-proof

Hyperammonemia induces mitochondrial dysfunction and neuronal cell death

Plamena R. Angelova, Annarein J.C. Kerbert, Abeba Habtesion, Andrew Hall, Andrey Y. Abramov, Rajiv Jalan

PII: S2589-5559(22)00082-9

DOI: https://doi.org/10.1016/j.jhepr.2022.100510

Reference: JHEPR 100510

To appear in: *JHEP Reports*

Received Date: 20 January 2022

Revised Date: 21 April 2022

Accepted Date: 10 May 2022

Please cite this article as: Angelova PR, Kerbert AJC, Habtesion A, Hall A, Abramov AY, Jalan R, Hyperammonemia induces mitochondrial dysfunction and neuronal cell death, *JHEP Reports* (2022), doi: https://doi.org/10.1016/j.jhepr.2022.100510.

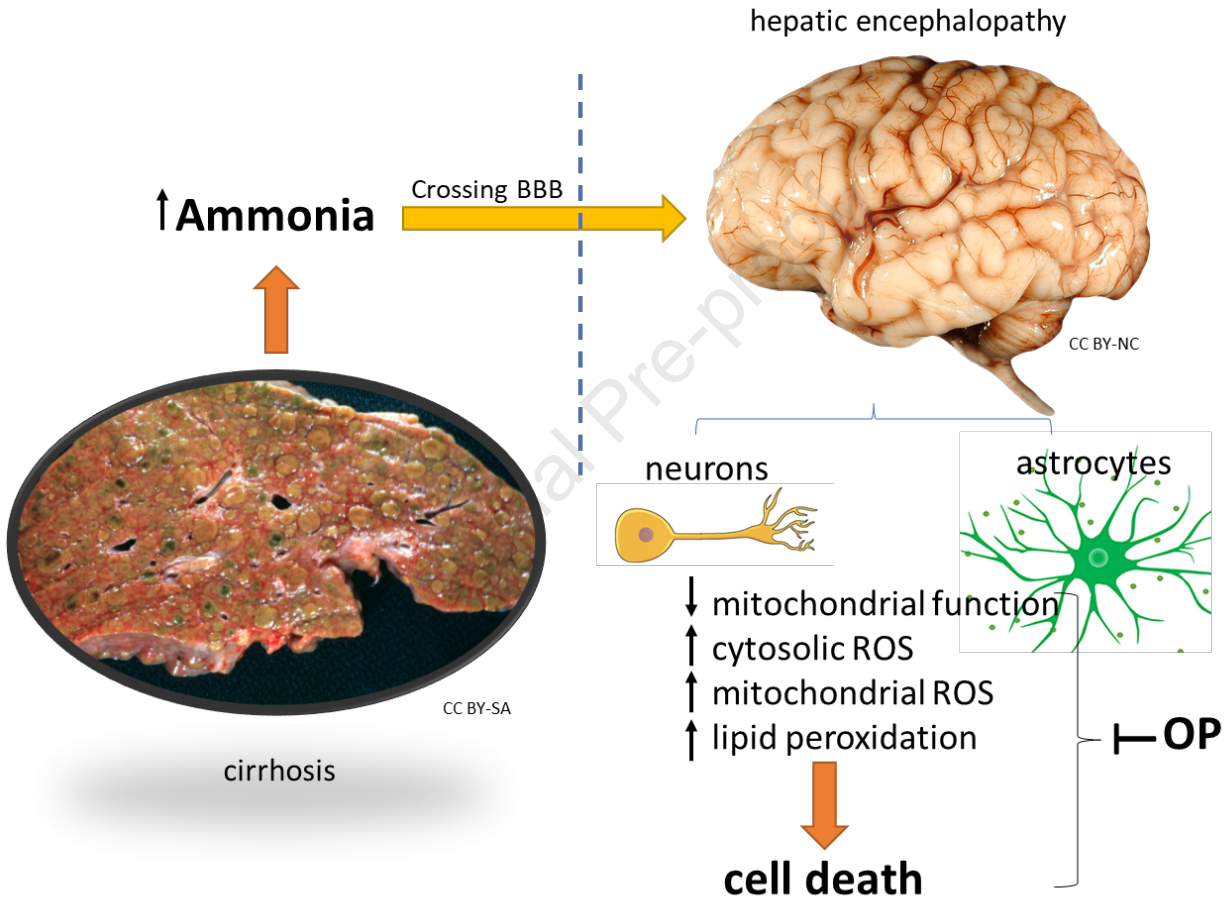
hepatic encephalopathy
↑Ammonia
Crossing BBB
CC BY-NC
neurons
astrocytes
↓ mitochondrial function
↑ cytosolic ROS
↑ mitochondrial ROS
↑ lipid peroxidation
⊢ OP
cell death
CC BY-SA
cirrhosis

HYPERAMMONEMIA INDUCES MITOCHONDRIAL DYSFUNCTION AND NEURONAL CELL DEATH

Plamena R. Angelova[1*] and Annarein J.C. Kerbert[2*], Abeba Habtesion[2], Andrew Hall[3], Andrey Y. Abramov[1#] and Rajiv Jalan[2,4#]

*Joint first authors

[#]Joint senior authors

[1]Queen Square Institute of Neurology, University College London, London, United Kingdom.

[2]Institute for Liver and Digestive Health, University College London, Royal Free Campus, London, United Kingdom.

[3]Sheila Sherlock Liver Centre, Royal Free London NHS Foundation Trust, London, UK.

[4]European Foundation for the Study of Chronic Liver Failure, Barcelona, Spain

Corresponding author: Rajiv Jalan, Institute for Liver and Digestive Health, University College London, Royal Free Campus, Rowland Hill Street, NW3 2PF, London, United Kingdom. Email: r.jalan@ucl.ac.uk; phone: +442074332845.

Keywords: liver cirrhosis, hepatic encephalopathy, ammonia, mitochondrial function, cell death

Electronic word count: 6083

Number of tables: 0; **Number of figures:** 6

Authors' contributions

P.R.A. - conceptualization, methodology, validation, formal analysis, investigation, data curation, visualization, writing - original draft preparation, review and editing;

A.J.K. - conceptualization, methodology, validation, formal analysis, investigation, data curation, writing - original draft preparation, review and editing;

A.H. - technical and experimental support, review and editing of the manuscript.

An.H. - technical and experimental support, review and editing of the manuscript.

A.Y.A - conceptualization, resources, supervision, writing - review and editing.

R.J. - conceptualization, resources, supervision, writing - review and editing.

Conflict of interest

P.R.A, A.J.K., A.H., An.H. and A.Y.A have no conflicts to declare.

R.J. - has research collaborations with Yaqrit and Takeda. He is the inventor of OPA which has been patented by University College London and licensed to Mallinckrodt Pharma. He is also a founder of Yaqrit limited, a spin out company from University College London. He has also co-founded Hepyx Ltd. and Cyberliver Ltd.

Financial support statement: Annarein J.C. Kerbert received funding from the European Association for the Study of the Liver (EASL).

Data availability statement: The data generated and analysed during the current study are included in this published article or available from the corresponding author upon reasonable request.

ABSTRACT

Background & Aims: In liver cirrhosis, astrocytic swelling is believed to be the principal mechanism of ammonia neurotoxicity leading to hepatic encephalopathy (HE). The role of neuronal dysfunction in HE is not clear. We aimed to explore the impact of hyperammonemia on mitochondrial function in primary co-cultures of neurons and astrocytes and in acute brain slices of cirrhotic rats using live cell imaging.

Methods: To primary co-cultures of astrocytes and neurons, low concentrations (1 and 5μM) of NH_4Cl were applied. In rats with bile-duct ligation (BDL)-induced cirrhosis, a model known to induce hyperammonemia and minimal HE, acute brain slices were studied. One group of BDL rats were treated twice daily with the ammonia scavenger ornithine phenylacetate (OP, 0.3g/kg). Fluorescence measurements of changes in mitochondrial membrane potential ($\Delta\Psi m$), cytosolic and mitochondrial reactive oxygen species (ROS) production, lipid peroxidation (LP) rates, and cell viability were performed using confocal microscopy.

Results: Neuronal cultures treated with NH_4Cl exhibited mitochondrial dysfunction, ROS overproduction and reduced cell viability (27.8±2.3% and 41.5±3.7%, respectively) compared to untreated cultures (15.7±1.0%, both $p<0.0001$). BDL led to increased cerebral LP ($p=0.0003$) and cytosolic ROS generation ($p<0.0001$), which was restored by OP (both $p<0.0001$). Mitochondrial function was severely compromised in BDL resulting in hyperpolarization of $\Delta\Psi m$ with consequent overconsumption of ATP and augmentation of mitochondrial ROS production. Administration of OP restored $\Delta\Psi m$. In BDL animals, neuronal loss was observed in hippocampal areas, which was partially prevented by OP.

Conclusions: Our results elucidate that low-grade hyperammonemia in cirrhosis can severely impact on brain mitochondrial function. Profound neuronal injury was

observed in hyperammonemic conditions, which was partially reversible by OP. This points towards a novel mechanism of HE development.

Word count: 275

Lay summary

The impact of hyperammonemia, a common finding in patients with liver cirrhosis, on brain mitochondrial function was investigated in this study. The results show that ammonia in concentrations commonly seen in patients induces severe mitochondrial dysfunction, overproduction of damaging oxygen molecules and profound injury and death of neurons in rat brain cells. These findings point towards a novel mechanism of ammonia-induced brain injury in liver failure and potential novel therapeutic targets.

Graphical abstract

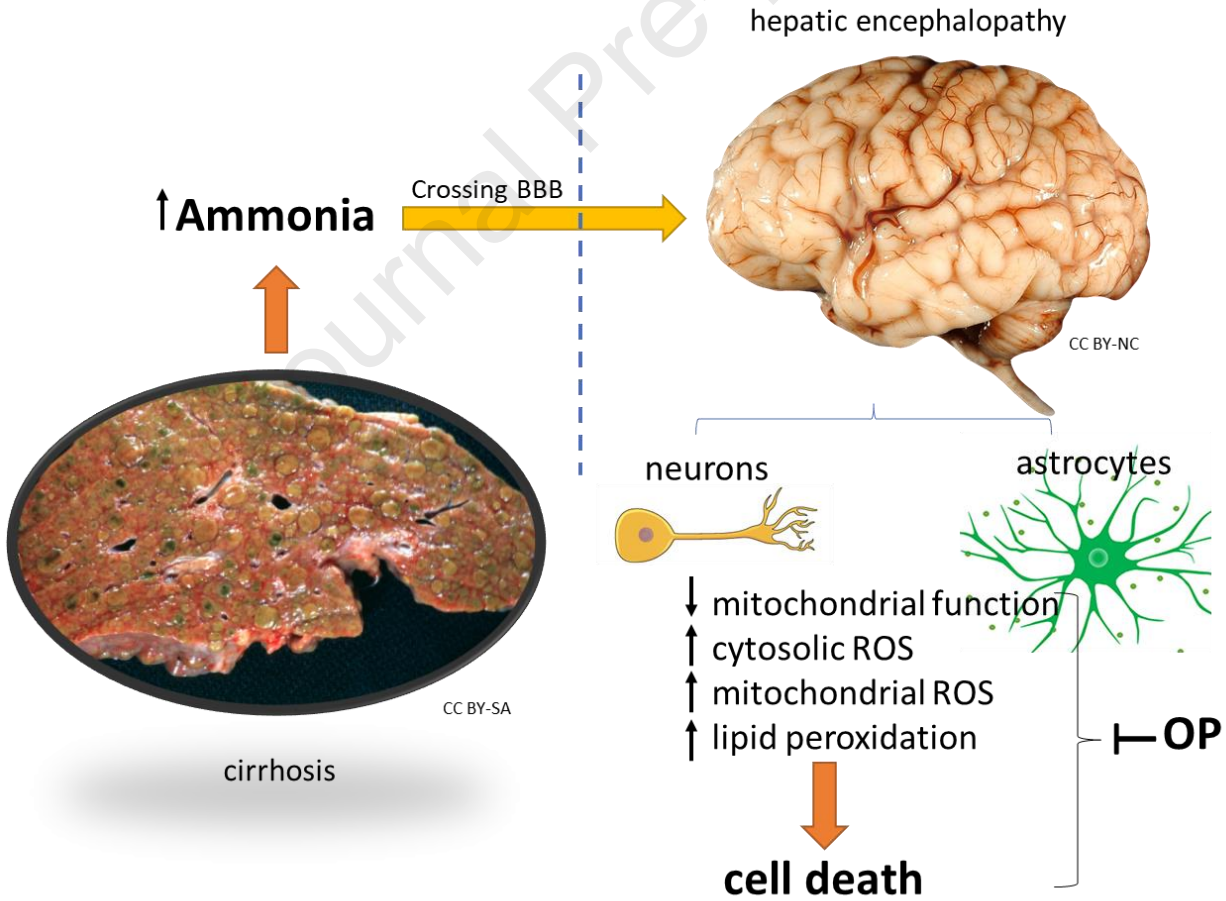

Highlights

- Low concentrations of ammonia induce mitochondrial dysfunction, overproduction of ROS and cell death in primary neurons.
- Hyperammonemia in cirrhotic rats leads to ROS and LP overproduction, which was prevented by the ammonia scavenger OP.
- In neurons from cirrhotic rats, hyperpolarization of ΔΨm was observed, which was restored by OP treatment.
- In a rat model of liver cirrhosis, profound neuronal loss was observed in the hippocampus.

INTRODUCTION

Hepatic encephalopathy (HE) is a severe complication of cirrhosis and manifests with a wide range of cognitive, psychiatric and motor system abnormalities (Vilstrup et al., 2014). In patients with liver failure, hepatic detoxification of ammonia via the urea cycle is impaired, which leads to increased ammonia levels in the circulation (Felipo, 2013). Ammonia in its gaseous form can freely pass the blood-brain barrier, where it is known to induce a variety of derangements in the central nervous system, including astrocyte swelling, brain oedema, neuroinflammation, increased glutamatergic neurotransmission and oxidative stress (Bemeur, Desjardins, & Butterworth, 2010; Felipo & Butterworth, 2002).

As the central nervous system (CNS) is highly dependent on mitochondrial energy supply in the form of adenosine triphosphate (ATP), alteration of energy balance of neurons that leads to energy deficit and oxidative stress ultimately initiates CNS injury and cell death (Abramov & Angelova, 2019b; Angelova & Abramov, 2018). In the last decade, studies have suggested a possible role for ammonia-induced mitochondrial dysfunction in the development of HE (Hertz & Kala, 2007; Skowronska & Albrecht, 2013), (Rao & Norenberg, 2001). The exact mechanism is not yet fully elucidated, but it includes glutamine-derived ammonia accumulation within the mitochondrial matrix of astrocytes, ammonia-induced inhibition of tricarboxylic acid (TCA) cycle enzymes, induction of mitochondrial permeability transition (mPT), impairment of electron transport chain complexes and induction of oxidative stress (Hertz & Kala, 2007; Rama Rao & Norenberg, 2012). However, the data from these studies are difficult to put into clinical context as almost all these studies have used *in-vitro* models with non-

physiologically high concentrations of ammonia and focussed almost entirely on the astrocytes (Heidari, 2019).

Brain energy metabolism is a well-balanced process that encompasses not only the processes of ATP production inside the cells, but also neuron-glia interactions (Abramov & Angelova, 2019b). Considering this, even if ammonia has a direct effect only on astrocytes, energy metabolism in neurons is unlikely to remain unaffected. Traditionally, HE has been thought to be reversible but emerging data clearly indicate that complete recovery of cognitive function is not consistently observed in patients with an episode of HE (Garcia-Martinez et al., 2011),(Sotil, Gottstein, Ayala, Randolph, & Blei, 2009), suggesting that neuronal dysfunction and cell death may be important in the pathogenesis of HE. In this study, we aimed to investigate the impact of low-grade hyperammonemia on mitochondrial function in neurons and astrocytes both *in-vitro* (primary co-cultures of neurons and astrocytes) and *ex-vivo* (acute brain slices) using live cell-imaging techniques. We have found that even disease-relevant concentrations of ammonia significantly alter mitochondrial metabolism of primary neurons, activates overproduction of reactive oxygen species (ROS) and oxidative stress that leads to neuronal cell death. Importantly, in acute brain slices of a rodent model of HE we also observed mitochondrial dysfunction, ROS overproduction and loss of neurons in different hippocampal areas. Importantly, ammonia-lowering treatment with Ornithine Phenylacetate (OP) led to the prevention of hyperpolarisation of the mitochondrial membrane potential ($\Delta\Psi m$) and reduced ROS production in neurons and thereby also had a neuroprotective effect.

MATERIALS AND METHODS

All experimental procedures were performed in compliance with the United Kingdom Animal (Scientific Procedures) Act of 1986 (updated 2012) and with the European directive 2010/63/EU, approved by the UCL Animal Welfare and Ethical Review Body under full project and establishment licenses (No.: 14378). Rats were group housed in individually ventilated cages and kept on a 12-hour light-dark cycle with ad libitum access to water and food.

Cell culture

Primary co-cultures of neurons and astrocytes were isolated from brains of Sprague-Dawley pups from the UCL breeding colony (P3-4) following the method described by Angelova et al. (Angelova et al., 2016) with few modifications. In brief, the brain was extracted, homogenized and dissociated with 0.25% trypsin-EDTA (Sigma Aldrich). The mixed neuron and astrocyte suspension was plated on pre-coated glass coverslips with Poly-D-lysine (1 mg/ml). Cells were maintained in Neurobasal with 2% of B27 (Invitrogen) and 2 mM L-glutamine, 1% of penicillin/streptomycin (Sigma-Aldrich). Cell cultures were maintained in a humidified incubator at 37°C and 5% CO_2.

As the in-vitro environment of neuronal cultures lacks important buffering and metabolic pathways, we decided to start with very low concentrations of NH_4Cl in the *in-vitro* studies (1 µM and 5 µM NH_4Cl) in order to prevent inducing cell death straight away before or during live cell imaging. Surprisingly, we found already an effect on mitochondrial function with these low concentrations. Therefore, we decided to proceed with these concentrations also in the *ex-vivo* brain slices studies, which showed consistent results.

To assess age-dependency of NH_4Cl effects two “age” groups were used: 7 days in vitro (DIV, i.e., immature cultures) and 16DIV (i.e., mature cultures). We have chosen to study these two time points, as we have shown in previous studies that there is a profound difference in mitochondrial bioenergetics between immature and mature neurons (Abramov & Duchen, 2010). Neurons were easily distinguishable from glia: they appeared phase bright, had smooth rounded somata and distinct processes, and laid just above the focal plane of the glial layer.

Rodent model of hepatic encephalopathy

In male Sprague-Dawley rats (age 8-10 weeks, weight ~300-450g), liver cirrhosis was induced by bile duct ligation (BDL) surgery, as described in (Harry et al., 1999). Rats were studied 4 weeks after BDL (N=5) or sham (N=5) operation. Of the BDL-operated rats, 2 rats were treated with the ammonia scavenging drug OP (0.3 g/kg intraperitoneally) twice daily during the last 5 days of the model.

Acute brain slices

Rats were sacrificed by neck dislocation under general anaesthesia (2% isoflurane in oxygen) after a cardiac perfusion with cold Ringer solution. Following decapitation, brains were rapidly removed and transverse slices (100 µm thick) were prepared using a Leica VT1200S vibratome. Slicing was performed in ice-cold solution that contained (in mM): 120 NaCl, 10 glucose, 2.5 KCl, 1.3 $MgSO_4$, 1 NaH_2PO_4, 1.3 $MgCl_2$, 2 $CaCl_2$, 10 HEPES, pH adjusted to 7.4. Once cut, slices were incubated at room temperature for one hour for recovery in the presence of fluorescent indicators.

Live cell imaging

Fluorescence measurements of changes in ΔΨm, mitochondrial ROS production, rate of lipid peroxidation (LP) and assessment of cell death were performed using a Zeiss 710 VIS CLSM equipped with a META detection system and a 40x oil immersion objective.

Mitochondrial membrane potential

Tetramethyl rhodamine, methyl ester (TMRM) is a cationic, cell-permeant fluorescent dye that was used to assess ΔΨm. The cells and slices were loaded with 25 nM TMRM for 40 min. Z-stacks were acquired using an excitation wavelength of 561 nm with a long pass filter and a 40x oil immersion objective.

Mitochondrial ROS production

For assessing mitochondrial ROS production, cells and slices were loaded with 1 µM MitoTracker Red CM-H2Xros (Thermo Scientific) and incubated for 20 min, after which the increase in fluorescence over time was imaged using 561 nm excitation and long pass filter. Confocal images were obtained using a 40x oil immersion objective.

Lipid peroxidation

For assessing the LP, cells and slices were loaded with 5 µM C11-BODIPY (581/591) for 30 min and washed. The dye was excited at 488 nm and 561 nm and detected using a 40x oil immersion objective. The ratio of 581/591 nm was analysed, and the rates were then calculated in A.U./min.

Cell death

For assessment of cell death *in-vitro*, cells were treated for 24 hours with 1 µM and 5 µM NH_4Cl. Prior to imaging, cells were incubated with propidium iodide (PI; 10 µM) and 300 nM Hoechst for 15 min, washed 3 times with PBS 1x and analysed using a cooled CCD camera. Hoechst stains the total number of nuclei while PI stains only cells with a disrupted plasma membrane. Dead cells (PI positive) were counted as a fraction of the total (Hoechst positive). In each experiment, five random fields were examined. The mean is representative for three independent experiments for each condition.

Cytosolic ROS production

Superoxide production was measured by using dihydroethidium (HEt; 5 µM, Invitrogen) in HBSS at room temperature. Fluorescent images were acquired using an inverted epifluorescence microscope, equipped with a 20x fluorite objective at a frame interval of 10 seconds. The ratio of oxidised and reduced forms of HEt was measured at 530 nm excitation and emission above 560 nm to allow quantification of the oxidised form (ethidium), whereas 380 nm excitation and emission from 405 to 470 was used to record the reduced form of the dye. Data were analysed using software from Andor IQ 3 (Belfast, UK).

NADH redox index and NADH pools

The autofluorescence of NADH and NADPH (which can be referred to NAD(P)H) was imaged on a cooled charge-coupled device (CCD) camera (Hamamatsu, Orca ER). The blue autofluorescence, emitted by the pyridine nucleotides NADH and NADPH in their reduced form, was excited using a 360 nm filter and emission was collected using

a 455 nm filter. Confocal images were acquired using a Zeiss 510 UV LSM system and a 40x objective. The application of 1 µM of the mitochondrial uncoupler carbonyl cyanide 4-(trifluoromethoxy) phenylhydrazone (FCCP) maximized the rate of respiration and oxidized the mitochondrial NADH pool in cells, resulting in a decrease of detected fluorescence (minimum = 0% for NADH). The subsequent application 1 mM of the complex IV inhibitor sodium cyanide (NaCN) suppressed respiration preventing NADH oxidation and allowing the NADH pool to be regenerated (maximum = 100% for NADH) (Cheng et al., 2020). Quantitative analysis of the obtained images was performed cell by cell using the Andor IQ3 software (Belfast, UK). The average was taken from n > 3 independent experiments for each condition.

Immunofluorescence

GFAP and beta-III Tubulin immunofluorescence staining was performed in paraffin-embedded brain tissue of the BDL rat model to stain respectively astrocytes and neurons. Tissue sections were dewaxed with xylene (15 mins x3) and hydrated through ethanol (2 mins x 3 to tap water). Sections were microwaved at 640W in 1L citrate buffer (10 mM Sodium Citrate, 0.05% Tween 20, pH 6.0) for 20 minutes, after which a protein block was applied (Abcam ab64226) for 10 minutes. Sections were then incubated in primary antibody with mouse Anti-beta III Tubulin (Abcam ab78078) and rabbit anti-GFAP antibody (Abcam ab7260), 1:200 and 1:1000 respectively diluted in antibody diluent (Agilent S080983-2). After incubation in the primary antibody, sections were washed in TBS pH 7.6 (5 mins) before application of secondary antibodies: goat anti-mouse IgG -Alexa Fluor 594 (ab150120) and goat anti-rabbit IgG -Alexa Fluor 647 (Abcam ab150079) both at 1:100 dilution diluted in TBS pH7.6 for 30 mins in the dark at room temperature. Sections were mounted in aqueous mounting

medium with DAPI (Abcam ab1044139). A multispectral image was taken of each slide using Akoya Mantra 2 imaging system. A 14-bit depth image was taken at 10 nm intervals between 400 and 720nm for each of 6 different filters, DAPI, CYP, FITC, CY3, TEXRED, CY5, CY7 and spectrally unmixed.

Immunoreactivity image analysis was performed using ImageJ software (1.51j8). Cell layer densities of the DG, CA1 and CA3 hippocampal regions of individual animals were calculated as the average densities of each region obtained from fifteen ROI per area per slice. Results are expressed as integrated density taken from the mean fluorescence intensity (in pixels) per μm^2.

Statistical analysis

Data were analysed with Origin Pro 2018 (MicroCal, Oregon, USA) and are expressed as mean ± SEM, N=number of animals and n=number of slices, unless otherwise stated. Two-tailed unpaired Student's *t*-test or one-way ANOVA followed by Bonferroni *post-hoc* test was used to estimate the statistical significance between experimental groups. Significance was accepted at a 95% confidence level ($p < 0.05$). * $p < 0.05$, ** $p < 0.001$, *** $p < 0.0001$.

RESULTS

Cell culture

Micromolar concentrations of ammonium chloride induced mitochondrial dysfunction in primary neurons

In a set of experiments in primary co-cultures, we were able to control for NH_4Cl delivered directly to neurons and astrocytes. The effect of 5 µM NH_4Cl was found to

be age dependent. First, we assessed ΔΨm, which is involved in most mitochondrial processes and can be taken as an indicator of mitochondrial health. In immature neurons (DIV7), application of NH_4Cl induced hyperpolarisation of the mitochondrial membrane (Figure 1, A1). In mature neurons (DIV16), however, application of NH_4Cl induced a profound mitochondrial depolarisation (Figure 1, A3).

NADH is a substrate and donor of electrons for complex I of mitochondria and changes in NADH autofluorescence can help estimate the activity of NADH-dependent respiration in living neurons and astrocytes. Application of 5 µM NH_4Cl to immature neurons induced a moderate increase in NADH autofluorescence (Figure 1 B1 and B3, from 2.67±1.45% to 8.03±3.36%, n=12, $p< 0.0001$) that may be explained by the activation of NADH production in the TCA cycle or by a mild inhibition of mitochondrial respiration. In mature primary neurons addition of 5 µM NH_4Cl induced a slow decrease in NADH autofluorescence. This, in combination with the data obtained for the ΔΨm, strongly suggests mitochondrial uncoupling (Figure 1 B 2-3, from 12.17±4.63% to 8.26±2.47%, n=18, p=0.0033).

Micromolar concentrations of ammonium chloride induced mitochondrial ROS production and oxidative stress in primary neurons

The effects of 5 µM exogenously applied NH_4Cl on mitochondrial ROS production also appeared to be dependent on age: immature neurons produced less mitochondrial and cytosolic ROS compared to mature neurons (mitochondrial: 23.93±5.88 vs. 70.30±48.91, n=9, p=0.0122; Figure 1 C1-2; cytosolic: 25.92±7.34 vs. 104.97±52.61, n=9, p=0.0057; Figure 1 D1-3). However, ROS production can play a physiological role and in cells with efficient antioxidant system it does not induce oxidative damage.

The LP rate, one of the hallmarks of oxidative stress, indicates possible damage to cell lipid composition that is involved in neuronal pathology. Importantly, 5μM NH_4Cl induced more activation of LP in mature neurons than in immature ones (0.0051±0.009 vs. 0.7428±0.091, p<0.0001; Figure 1 E1-3). Thus, micromolar concentrations of ammonia induced overproduction of ROS in mitochondria and the cytosol, which led to LP and oxidative stress.

Acute brain slices

We have previously shown in large numbers of sham (n=22), BDL (n=26) and BDL+OP treated (n=14) Sprague-Dawley rats, that BDL rats have significantly higher plasma ammonia levels, as compared to sham (141±4 μmol/L vs. 56±3 μmol/L, p<0.001), which is normalized by OP treatment (60±2 umol/L, Supplementary table 1) (Hadjihambi et al., 2017).

Hyperammonemia leads to hyperpolarisation of brain mitochondria

Using TMRM as a fluorescent indicator for ΔΨm in acute brain slices we observed that hyperammonemia led to hyperpolarisation of mitochondria (sham: 2181.64±90.76, n=14, vs. BDL: 3482.00±554.44, n=15, p<0.0001; Figure 2 B, C1-C2). Scavenging of the ammonia by administration of OP to BDL animals, effectively reduced ΔΨm in acute brain slices. Interestingly, OP-treated BDL animals had even lower ΔΨm values than sham animals (Figure 2 B, C3, from 3482.00±143.16, n=15 for BDL to 1205.39±99.63, n=23 for BDL+OP, p<0.0001).

Hyperpolarisation or depolarisation of mitochondria was induced by various triggers. In order to understand the mechanism of the effect of BDL on mitochondrial function

we applied several mitochondrial toxins (i.e., oligomycin, rotenone, FCCP) in the TMRM measurements. As expected, application of 2 µg/ml oligomycin, an inhibitor of ATP synthase/ATPase, had no effect on ΔΨm in sham animals (Figure 2 C1, n=14). Application of the complex-I inhibitor rotenone (5 µM) induced complete mitochondrial depolarisation and the uncoupler FCCP (1 µM) did not induce a further decrease in TMRM fluorescence. This strongly suggests that ΔΨm of the cells in these brain slices are exclusively maintained by the electron transport chain (ETC) of mitochondria. In acute brain slices from BDL rats, application of oligomycin induced a 25% decrease in ΔΨm (Figure 2 C2, n=15) suggesting that due to dysfunction in ETC, ΔΨm is maintained by the consumption of ATP in the ATPase instead of its production. However, rotenone still induced a profound decrease in TMRM fluorescence, indicating that part of the ΔΨm is still maintained by the ETC. Such combination of mitochondrial respiration and ATPase activity leads to pathological mitochondrial hyperpolarisation (Abramov & Duchen, 2010; Abramov et al., 2010; Esteras, Rohrer, Hardy, Wray, & Abramov, 2017). Importantly, administration of OP led to recovery of the response to oligomycin, but this was not sufficient to restore the ΔΨm to control levels (Figure 2 C3, n=23).

Hyperammonemia led to overproduction of ROS in neuronal mitochondria

Hyperpolarisation of mitochondria in combination with altered mechanism of ΔΨm maintenance can lead to the activation of ROS generation in the ETC (Abramov et al., 2010; Angelova & Abramov, 2018; Esteras et al., 2017). To test if increased ΔΨm in BDL rats can trigger ROS production, we measured the rate of mitochondrial ROS production in acute brain slices using MitoTracker ROS. The rate of mitochondrial ROS production in brain slices from BDL rats was 2.6 times higher than in those of

control rats (205.3±21.8, n=9, for control vs. 487.1±44.64 for BDL, n=12, p<0.0001; Figure 3 A, B, C1-C2). Importantly, administration of OP reduced the production of ROS in mitochondria from BDL rats to levels seen in the controls (from 487.1±44.64, n=12, for BDL to 162.6±36.6, n=8, for BDL+OP, p<0.0001).

Hyperammonemia induces intracellular ROS overproduction

Mitochondria are just one of the multiple sources of ROS production in brain cells. Additionally, mitochondria produce superoxide anion and hydrogen peroxide into the matrix and the cytosol (Angelova & Abramov, 2016). We found that BDL-induced hyperammonemia led to a more than 3-fold increase in cytosolic ROS generation rates (218.4±67.6, n=9, for control vs. 926.0±67.7, n=8, for BDL, p<0.0001; Figure 4 A, B, C1-C2), which was attenuated by OP treatment (474.9±48.8, n=11, p<0.0001; Figure 4 B, C3). Changes in the rate of ROS production from various exogenous or endogenous sources may play a role in redox signalling and have beneficial effects on cells (Sokolovski, Rafailov, Abramov, & Angelova, 2021). To investigate whether hyperammonemia-induced ROS production in brain cells triggers pathological oxidative stress, we measured the rate of LP.

Hyperammonemia increases the rate of lipid peroxidation and induces oxidative stress in the brain

The rate of LP in acute brain slices was assessed using radiometric fluorescent indicator C-11 BODYPY (Figure 5 A). In agreement with the results on ROS generation measurements, BDL-induced hyperammonemia led to a significant increase in the rate of LP (0.047±0.006, n=7, for Sham vs. 0.084±0.019, n=9, for BDL, p=0.0003; Figure 5 B, C1-C2). OP treatment efficiently protected the cells against LP (0.084±0.006, n=9,

for BDL compared to 0.032±0.006, n=8, for BDL+OP, p<0.0001; Figure 5 B, C3). Thus, hyperammonemia-induced overproduction of ROS in mitochondria and cytosol induced oxidative stress.

In vitro and *ex vivo* evidence of neuronal cell death

Oxidative stress induced by overproduction of mitochondrial ROS eventually results in mitochondrial dysfunction and initiation of the process of cell death and neurodegeneration (Angelova & Abramov, 2018). To assess this, neuronal cultures (16 DIV) were pre-treated with low doses of NH_4Cl (1 µM and 5 µM over 24 h). Cultures pre-treated with 1 µM or 5 µM NH_4Cl were found to indeed exhibit reduced cell viability (Figure 6 A-B, 27.8±2.3 %, n=10, and 41.5±3.7 %, n=10, respectively) compared to untreated cultures (15.7±1.0 %, n=11, both p<0.0001).

Ex vivo cell density was assessed using immunofluorescence staining of neurons (labelled with beta-III-tubulin) and astrocytes (GFAP-labelled) in the temporal lobe of the rat brains, i.e. the hippocampal areas DG (dentate gyrus), CA1 (cornu ammonis 1) and CA3 (cornu ammonis 3). Significant neuronal loss was evident in all three areas: DG (2.68±1.09%, n=15 vs. 11.48±0.99%, n=15 for control, p<0.0001), in CA1 (6.03±0.61%, n=15 vs. 12.03±1.25%, n=15 for control, p<0.0001) and in the CA3 (8.07±0.60%, n=15 vs. 13.77±1.06%, n=15 for control, p<0.0001) at 1-month post-BDL (Figure 6 B,C, left and central panel columns). This neuronal loss was significantly ameliorated by OP treatment in the DG (10.83±0.76%, n=15 vs. 2.68±1.09±%, n=15 for BDL, p<0.0001) and the CA1 (11.19±1.28%, n=15 vs. 6.03±0.61%, n=15 for BDL, p<0.0001) areas of the hippocampus (Figure 6, right panel columns), but was not statistically significant in the CA3 area (n=15, p=0.3378).

Significant increase in the number of GFAP-positive astroglial cells was observed 1-month post-BDL in the DG (5.51±0.39%, n=15 vs. 2.68±0.37%, n=15 for control, $p<0.0001$) as well as in the CA3 (4.51±0.47%, n=15 vs. 2.47±0.26%, n=15 for control, $p<0.0001$) areas, but not in the CA1 area (Figure 6 B,C, left and central panels). It must be noted that reactive astrogliosis and glial scar formation was evident in the BDL brains. This effect on the astrocytes was only slightly affected by OP treatment (Figure 6 B, C right side panels).

DISCUSSION

This study was designed to evaluate the role of pathophysiologically relevant concentrations of ammonia on neuronal viability and the role of mitochondrial dysfunction and oxidative stress in neuronal toxicity in *ex-vivo* brain slices from models of cirrhosis and in co-cultures of primary astrocytes and neurons. Our results strongly indicate that even low concentrations of ammonia (1-5 μM) can induce cell death in neurons (Figure 6A). Importantly, also in an established animal model of low-grade hyperammonemia (Lima, Miranda, Ferreira, Rachid, & Simoes, 2019), striking neuronal loss was observed in the hippocampal areas. Besides astrocyte swelling, profound neuronal injury and cell death were observed in cirrhotic rats. This might explain the recent observations suggesting that brain dysfunction following episodes of HE are not fully reversible (Garcia-Martinez et al., 2011), (Sotil et al., 2009). Our data underline the importance of early and targeted ammonia-lowering therapies in clinical practice and point to brain mitochondria as a potential novel therapeutic target in HE.

In both *in-vitro* and *ex-vivo* studies, we have shown that hyperammonemia induces mitochondrial hyperpolarization, increases ROS production and induces LP. This is in agreement with previous studies that have shown that hyperammonemia leads to increased generation of ROS in astrocytes (Skowronska & Albrecht, 2013), (Norenberg, 2003), (Norenberg, Jayakumar, & Rama Rao, 2004), which is likely due to ammonia-induced suppression of antioxidant enzymes such as catalase, glutathione peroxidase and superoxide dismutase (Kosenko et al., 1998; Murthy, Rama Rao, Bai, & Norenberg, 2001) and interruption of astrocytic glutathione synthesis (Bender, Reichelt, & Norenberg, 2000). Hyperammonemia and oxidative stress may lead to an increase in cytoplasmic Ca^{2+}, which affects mitochondrial function by inducing mitochondrial permeability transition, collapse of $\Delta\Psi m$, osmotic swelling of mitochondrial matrix, uncoupling of oxidative phosphorylation and interruption of ATP synthesis (Angelova, 2021), (Duchen, 2000), (Ermak & Davies, 2002). It should be noted that neurons and glial cells have differences in mitochondrial metabolism and in redox balance. However, astrocytic dysfunction can lead to alteration in neuronal mitochondrial metabolism and in the production of major antioxidants that also can have implications for neuronal cell death (Abramov & Angelova, 2019a).

Most of the evidence for these previous observations were obtained in cellular models of hyperammonemia. In this study, we have shown consistent results in a well-established, clinically-relevant rodent model of minimal/ non-overt HE (Butterworth et al., 2009). By applying live cell imaging techniques in the acute brain slices, the pathophysiological situation in these animals is very closely mimicked. Therefore, these data suggest that even when HE is not clinically evident, brain mitochondrial

function is severely impaired. This is supported by our observations in mature co-cultures of astrocytes and neurons, in which application of a very low concentration of NH_4Cl (5μM) led to increased ROS production, LP, and a ΔΨm collapse. These are important observations, as novel treatments targeting mitochondria may be of benefit in minimal/ non-overt HE and thereby potentially prevent the progression to overt HE.

The effect of micromolar concentrations of ammonia on mitochondrial metabolism of neurons was dependent on the age of the primary cell cultures. Thus, the mechanisms of these effects were different – from inhibition of the mitochondrial respiration (NADH consumption) to mitochondrial uncoupling (Figure 1). Differences in the effects between mature and immature neurons in culture can be possibly explained by the expression of the receptors in more mature neurons but more likely by the difference in the rate of ATP production and consumption in immature neurons (Abramov & Duchen, 2010). This finding provides a possible explanation for the clinical observation that older age is an independent risk factor for the development of HE (Tapper, Henderson, Parikh, Ioannou, & Lok, 2019).

Another important observation in the present study was that of hyperammonemia-induced neuronal loss. In the BDL model, we found significant neuronal loss in all three areas of the hippocampus: DG, CA1 and CA3 regions of the brain, which was consistent with the observation of reduced cell viability in the neuronal cell-cultures treated with NH_4Cl. Most studies investigating hyperammonemia-induced brain mitochondrial dysfunction have focussed on astrocytes, as these are traditionally thought to be the major cell type involved in brain ammonia metabolism. Our novel observation suggests that ammonia directly induces neuronal cell death, even at very

low concentrations and in the rodent model of minimal HE. It was intriguing to note that although ammonia-lowering treatment with OP led to recovery of mitochondrial function in the acute brain slice studies, there was a persistence of neuronal injury and cell death supporting the previous observations that HE is not completely reversible.

This study has a few limitations that should be considered. Firstly, we were not able to measure plasma ammonia levels in the BDL rat model. This was due to the fact that preparation of the acute brain slices does not allow the withdrawal of a clean, non-haemolyzed blood sample. However, we have extensive experience with this BDL model, including OP treatment. Ammonia levels of large numbers of animals included in an identically performed BDL model have been previously published (Hadjihambi et al., 2017) (Supplementary table 1) and showed small standard deviations. Secondly, the number of animals included in the current study was relatively low. Nevertheless, in keeping with the principles of the ARRIVE and 3Rs guidelines, it was considered unethical to proceed with inclusion of more animals as highly statistically significant differences between groups were already observed. Finally, this study was not designed to investigate the underlying mechanisms of hyperammonemia-induced ROS production, LP and $\Delta\Psi m$. Further studies are needed to explore this and to identify specific therapeutic targets to protect mitochondrial function during hyperammonemia.

In conclusion, this study makes the novel observation that low-grade hyperammonemia and minimal HE are associated with significant brain mitochondrial dysfunction, which results in increased ROS production, LP and ultimately in neuronal cell death. In addition, significant neuronal loss was observed in an animal model of

cirrhosis with low-grade hyperammonemia, which is only partially restored by correction of ammonia levels. These findings point towards the need for novel treatments targeting mitochondrial dysfunction, even in low-grade hyperammonemia and minimal HE.

ABBREVIATIONS

ATP, adenosine triphosphate; BDL, bile-duct ligation; CNS, central nervous system; DIV, days in-vitro; FCCP, carbonyl cyanide 4-(trifluoromethoxy) phenylhydrazone; HE, hepatic encephalopathy; LP, lipid peroxidation; mPT, mitochondrial permeability transition; NaCN, sodium cyanide; OP, ornithine phenylacetate; ROS, reactive oxygen species; TCA, tricarboxylic acid enzymes; ΔΨm, mitochondrial membrane potential

ACKNOWLEDGEMENTS

We thank Dr. Olga Kopach for hosting the animals at the QSH animal facility and for help with handling the animals for preparation for experiments (Schedule 1 and perfusion).

FIGURE LEGENDS

Figure. 1. Age-dependent NH_4Cl effect on mitochondrial function and oxidative status of primary cultures. **A,** Kinetic changes in ΔΨm from immature (A1) and mature (A3) rat primary neurons. Representative TMRM images before and 8' after application of 5μM NH_4Cl in immature (A2) and mature (A4) primary neurons. **B**, Changes in mitochondrial respiration of immature (A1) and mature (A1) rat neurons upon application of 5μM NH_4Cl. A3, Quantification bar-chart of the results in A1 and A2 (Im, immature; **M**, mature). **C,** Age-dependent mitochondrial ROS production. Representative traces (C1) and quantification bar-chart of basal rate of mitochondrial ROS generation rate (C2). **D,** Cytosolic ROS production in immature (D1) and mature (D2) primary rat neurons. Quantification of the results (D3) from D1 and D2 (Im, immature; M, mature). **E,** Lipid peroxidation in immature (E1) and in mature (E2) neurons from rat primary culture. Quantification of the results (E3) from E1 and E2 (Im, immature; M, mature). Scale bar = 50 μm. Data are represented as mean ± SEM. * $p < 0.05$, ** $p < 0.001$, *** $p < 0.0001$.

Figure. 2. BDL is associated with hyperpolarization of ΔΨm, which is restored by OP treatment. A, Representative images of TMRM fluorescence in acute brain slices from Sham operated, BDL and BDL/OP rats. **B,** Quantification bar-chart of ΔΨm in acute slices from Sham operated, BDL and BDL/OP rats. **C,** representative traces of dynamic changes of TMRM intensity from Sham operated (C1), BDL (C2) and BDL/OP (C3) rat brain slices upon application of oligomycin (2μg/ml), rotenone (1 μM) and fccp (1 μM). Scale bar = 50 μm. Data are represented as mean ± SEM. * $p < 0.05$, ** $p < 0.001$, *** $p < 0.0001$.

Figure. 3. Mitochondrial ROS production is increased in BDL and mitigated by OP. A, Representative images of MitoTracker Red CM-H2Xros fluorescence in acute slices from Sham operated, BDL and BDL/OP rats. **B,** Quantification bar-chart of mitochondrial ROS production rate in acute slices from Sham operated, BDL and BDL/OP rats. **C,** representative traces of several ROIs of MitoTracker Red CM-H2Xros intensity from Sham operated (C1), BDL (C2) and BDL/OP (C3) brain slices. Scale bar = 50 µm. Data are represented as mean ± SEM. * $p < 0.05$, ** $p < 0.001$, *** $p < 0.0001$.

Figure. 4. Cytosolic ROS production is elevated in BDL and alleviated by OP. A, Representative images of dihydroethidium (HEt) fluorescence in acute slices from Sham operated, BDL and BDL/OP rats. **B,** Quantification bar-chart of superoxide production rate in acute slices from Sham operated, BDL and BDL/OP rats. **C,** representative traces of several ROIs of HEt intensity at 530 nm from Sham operated (C1), BDL subjected (C2) and BDL/OP (C3) slices. Scale bar = 50 µm. Data are represented as mean ± SEM. * $p < 0.05$, ** $p < 0.001$, *** $p < 0.0001$.

Figure. 5. LP rate in acute slice of BDL rats is attenuated by OP. A, Images of C11-Bodipy acute slices (**red**, non-oxidised; **green** oxidised tissue) from Sham operated, BDL and BDL/OP rats. **B,** Quantification bar-chart of LP rate in acute slices from Sham operated, BDL subjected and BDL/OP rats. **C,** mean representative traces of C11-Bodipy ratio from Sham operated (C1), BDL subjected (C2) and BDL/OP (C3) slices. Scale bar = 50 µm. Data are represented as mean ± SEM. * $p < 0.05$, ** $p < 0.001$, *** $p < 0.0001$.

Figure. 6. Cell death in *in vitro* and *ex vivo* models of hyperammonemia. A, cell death rate assessed in primary co-culture of neurons and astrocytes upon application of low (1uM) and high (5uM) concentrations of NH_4Cl. Red (propidium iodide, non-viable cells) and blue (Hoechst, total number of cells). **B**, Immunostaining of neurons and astrocytes of fixed brain slices from Sham operated and animals subjected to BDL and to BDL/OP from DG, CA1 and CA3 areas from the rat hippocampus. Green (GFAP, glial fibrillary acidic protein, astrocytic marker), red (beta-III-tubulin, neuronal marker) and blue (DAPI, cell nuclei). Scale bar = 250 μm. **C,** Inset**:** schematic overview of the areas in rat hippocampus. Quantification bar charts for cell density in the DG, CA1 and CA3 for both neurons (left chart) and astrocytes (right chart). Data are represented as mean ± SEM. * $p < 0.05$, ** $p < 0.001$, *** $p < 0.0001$.

References

Author names in bold designate shared co-first authorship.

Abramov, A. Y., & Angelova, P. R. (2019a). Cellular mechanisms of complex I-associated pathology. *Biochem Soc Trans, 47*(6), 1963-1969. doi:10.1042/BST20191042

Abramov, A. Y., & Angelova, P. R. (2019b). Mitochondrial dysfunction and energy deprivation in the mechanism of neurodegeneration. *Turkish Journal of Biochemistry*. doi:https://doi.org/10.1515/tjb-2019-0255

Abramov, A. Y., & Duchen, M. R. (2010). Impaired mitochondrial bioenergetics determines glutamate-induced delayed calcium deregulation in neurons. *Biochim Biophys Acta, 1800*(3), 297-304. doi:10.1016/j.bbagen.2009.08.002

Abramov, A. Y., Smulders-Srinivasan, T. K., Kirby, D. M., Acin-Perez, R., Enriquez, J. A., Lightowlers, R. N., . . . Turnbull, D. M. (2010). Mechanism of neurodegeneration of neurons with mitochondrial DNA mutations. *Brain, 133*(Pt 3), 797-807. doi:10.1093/brain/awq015

Angelova, P. R. (2021). Sources and triggers of oxidative damage in neurodegeneration. *Free Radic Biol Med, 173*, 52-63. doi:10.1016/j.freeradbiomed.2021.07.003

Angelova, P. R., & Abramov, A. Y. (2016). Functional role of mitochondrial reactive oxygen species in physiology. *Free Radic Biol Med, 100*, 81-85. doi:10.1016/j.freeradbiomed.2016.06.005

Angelova, P. R., & Abramov, A. Y. (2018). Role of mitochondrial ROS in the brain: from physiology to neurodegeneration. *FEBS Lett, 592*(5), 692-702. doi:10.1002/1873-3468.12964

Angelova, P. R., Ludtmann, M. H., Horrocks, M. H., Negoda, A., Cremades, N., Klenerman, D., . . . Abramov, A. Y. (2016). Ca2+ is a key factor in alpha-synuclein-induced neurotoxicity. *J Cell Sci, 129*(9), 1792-1801. doi:10.1242/jcs.180737

Bemeur, C., Desjardins, P., & Butterworth, R. F. (2010). Evidence for oxidative/nitrosative stress in the pathogenesis of hepatic encephalopathy. *Metab Brain Dis, 25*(1), 3-9. doi:10.1007/s11011-010-9177-y

Bender, A. S., Reichelt, W., & Norenberg, M. D. (2000). Characterization of cystine uptake in cultured astrocytes. *Neurochem Int, 37*(2-3), 269-276. doi:10.1016/s0197-0186(00)00035-8

Butterworth, R. F., Norenberg, M. D., Felipo, V., Ferenci, P., Albrecht, J., Blei, A. T., & Members of the, I. C. o. E. M. o. H. E. (2009). Experimental models of hepatic encephalopathy: ISHEN guidelines. *Liver Int, 29*(6), 783-788. doi:10.1111/j.1478-3231.2009.02034.x

Cheng, X., Vinokurov, A. Y., Zherebtsov, E. A., Stelmashchuk, O. A., Angelova, P. R., Esteras, N., & Abramov, A. Y. (2020). Variability of mitochondrial energy balance across brain regions. *J Neurochem*. doi:10.1111/jnc.15239

Duchen, M. R. (2000). Mitochondria and calcium: from cell signalling to cell death. *J Physiol, 529 Pt 1*, 57-68. doi:10.1111/j.1469-7793.2000.00057.x

Ermak, G., & Davies, K. J. (2002). Calcium and oxidative stress: from cell signaling to cell death. *Mol Immunol, 38*(10), 713-721. doi:10.1016/s0161-5890(01)00108-0

Esteras, N., Rohrer, J. D., Hardy, J., Wray, S., & Abramov, A. Y. (2017). Mitochondrial hyperpolarization in iPSC-derived neurons from patients of FTDP-17 with

10+16 MAPT mutation leads to oxidative stress and neurodegeneration. *Redox Biol, 12*, 410-422. doi:10.1016/j.redox.2017.03.008

Felipo, V. (2013). Hepatic encephalopathy: effects of liver failure on brain function. *Nat Rev Neurosci, 14*(12), 851-858. doi:10.1038/nrn3587

Felipo, V., & Butterworth, R. F. (2002). Neurobiology of ammonia. *Prog Neurobiol, 67*(4), 259-279. doi:10.1016/s0301-0082(02)00019-9

Garcia-Martinez, R., Rovira, A., Alonso, J., Jacas, C., Simon-Talero, M., Chavarria, L., . . . Cordoba, J. (2011). Hepatic encephalopathy is associated with posttransplant cognitive function and brain volume. *Liver Transpl, 17*(1), 38-46. doi:10.1002/lt.22197

Hadjihambi, A., De Chiara, F., Hosford, P. S., Habtetion, A., Karagiannis, A., Davies, N., . . . Jalan, R. (2017). Ammonia mediates cortical hemichannel dysfunction in rodent models of chronic liver disease. *Hepatology, 65*(4), 1306-1318. doi:10.1002/hep.29031

Harry, D., Anand, R., Holt, S., Davies, S., Marley, R., Fernando, B., . . . Moore, K. (1999). Increased sensitivity to endotoxemia in the bile duct-ligated cirrhotic Rat. *Hepatology, 30*(5), 1198-1205. doi:10.1002/hep.510300515

Heidari, R. (2019). Brain mitochondria as potential therapeutic targets for managing hepatic encephalopathy. *Life Sci, 218*, 65-80. doi:10.1016/j.lfs.2018.12.030

Hertz, L., & Kala, G. (2007). Energy metabolism in brain cells: effects of elevated ammonia concentrations. *Metab Brain Dis, 22*(3-4), 199-218. doi:10.1007/s11011-007-9068-z

Kosenko, E., Kaminsky, Y., Lopata, O., Muravyov, N., Kaminsky, A., Hermenegildo, C., & Felipo, V. (1998). Nitroarginine, an inhibitor of nitric oxide synthase, prevents changes in superoxide radical and antioxidant enzymes induced by ammonia intoxication. *Metab Brain Dis, 13*(1), 29-41. doi:10.1023/a:1020626928259

Lima, L. C. D., Miranda, A. S., Ferreira, R. N., Rachid, M. A., & Simoes, E. S. A. C. (2019). Hepatic encephalopathy: Lessons from preclinical studies. *World J Hepatol, 11*(2), 173-185. doi:10.4254/wjh.v11.i2.173

Murthy, C. R., Rama Rao, K. V., Bai, G., & Norenberg, M. D. (2001). Ammonia-induced production of free radicals in primary cultures of rat astrocytes. *J Neurosci Res, 66*(2), 282-288. doi:10.1002/jnr.1222

Norenberg, M. D. (2003). Oxidative and nitrosative stress in ammonia neurotoxicity. *Hepatology, 37*(2), 245-248. doi:10.1053/jhep.2003.50087

Norenberg, M. D., Jayakumar, A. R., & Rama Rao, K. V. (2004). Oxidative stress in the pathogenesis of hepatic encephalopathy. *Metab Brain Dis, 19*(3-4), 313-329. doi:10.1023/b:mebr.0000043978.91675.79

Rama Rao, K. V., & Norenberg, M. D. (2012). Brain energy metabolism and mitochondrial dysfunction in acute and chronic hepatic encephalopathy. *Neurochem Int, 60*(7), 697-706. doi:10.1016/j.neuint.2011.09.007

Rao, K. V., & Norenberg, M. D. (2001). Cerebral energy metabolism in hepatic encephalopathy and hyperammonemia. *Metab Brain Dis, 16*(1-2), 67-78. doi:10.1023/a:1011666612822

S**kowronska, M., & Albrecht, J.** (2013). Oxidative and nitrosative stress in ammonia neurotoxicity. *Neurochem Int, 62*(5), 731-737. doi:10.1016/j.neuint.2012.10.013

Sokolovski, S. G., Rafailov, E. U., Abramov, A. Y., & Angelova, P. R. (2021). Singlet oxygen stimulates mitochondrial bioenergetics in brain cells. *Free Radic Biol Med, 163*, 306-313. doi:10.1016/j.freeradbiomed.2020.12.022

Sotil, E. U., Gottstein, J., Ayala, E., Randolph, C., & Blei, A. T. (2009). Impact of preoperative overt hepatic encephalopathy on neurocognitive function after liver transplantation. *Liver Transpl, 15*(2), 184-192. doi:10.1002/lt.21593

Tapper, E. B., Henderson, J. B., Parikh, N. D., Ioannou, G. N., & Lok, A. S. (2019). Incidence of and Risk Factors for Hepatic Encephalopathy in a Population-Based Cohort of Americans With Cirrhosis. *Hepatol Commun, 3*(11), 1510-1519. doi:10.1002/hep4.1425

Vilstrup, H., Amodio, P., Bajaj, J., Cordoba, J., Ferenci, P., Mullen, K. D., . . . Wong, P. (2014). Hepatic encephalopathy in chronic liver disease: 2014 Practice Guideline by the American Association for the Study of Liver Diseases and the European Association for the Study of the Liver. *Hepatology, 60*(2), 715-735. doi:10.1002/hep.27210

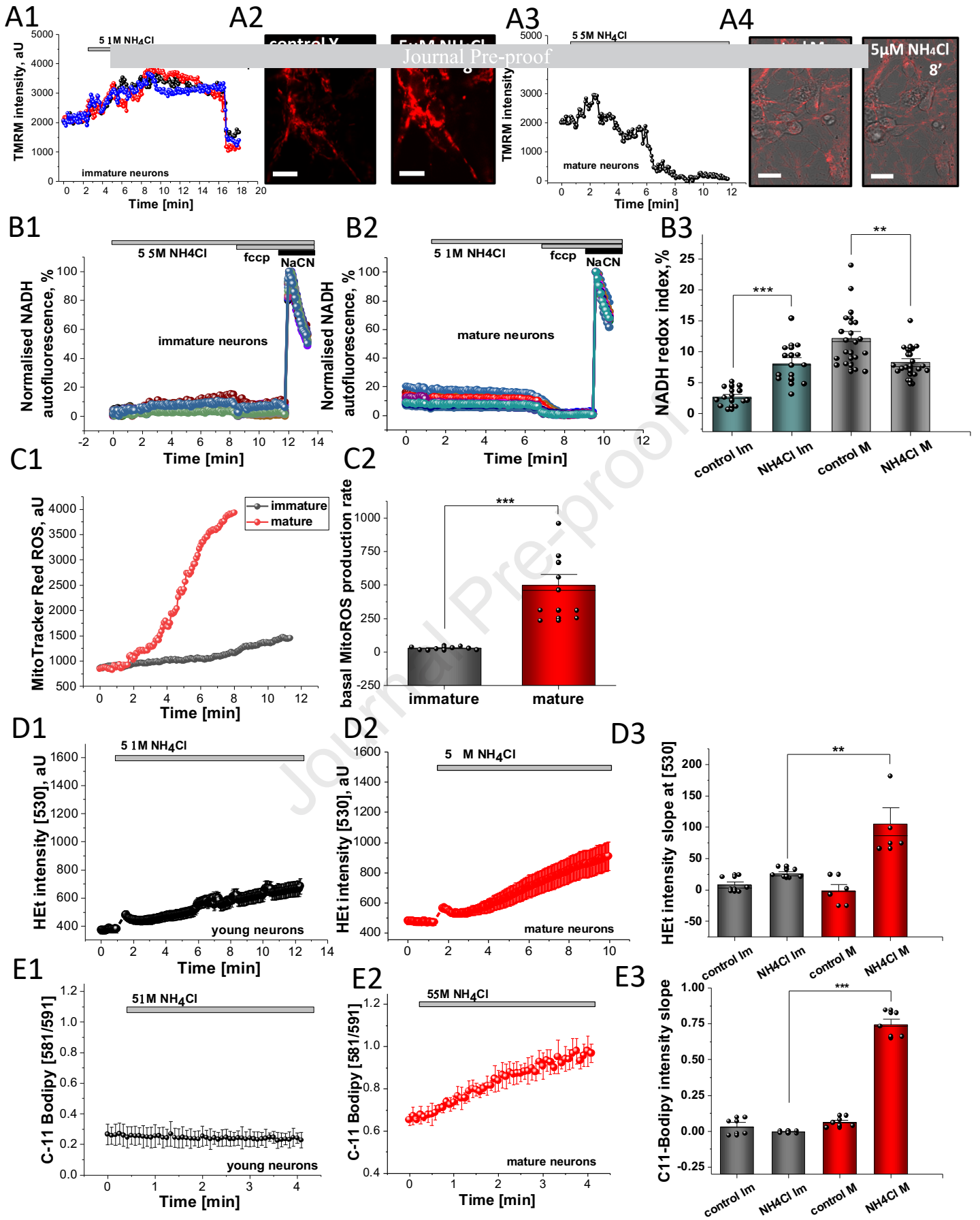

Figure 1.

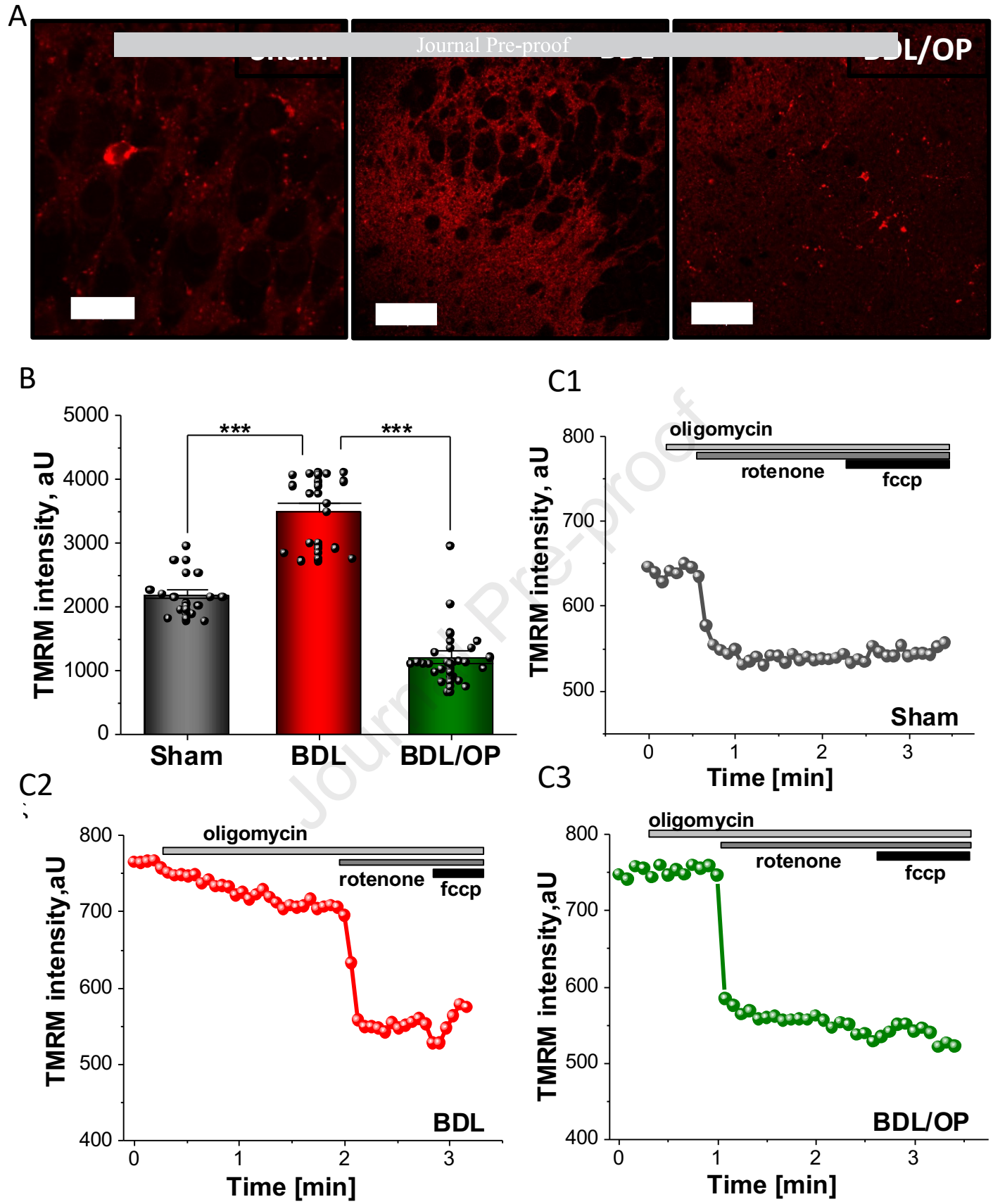

Figure 2.

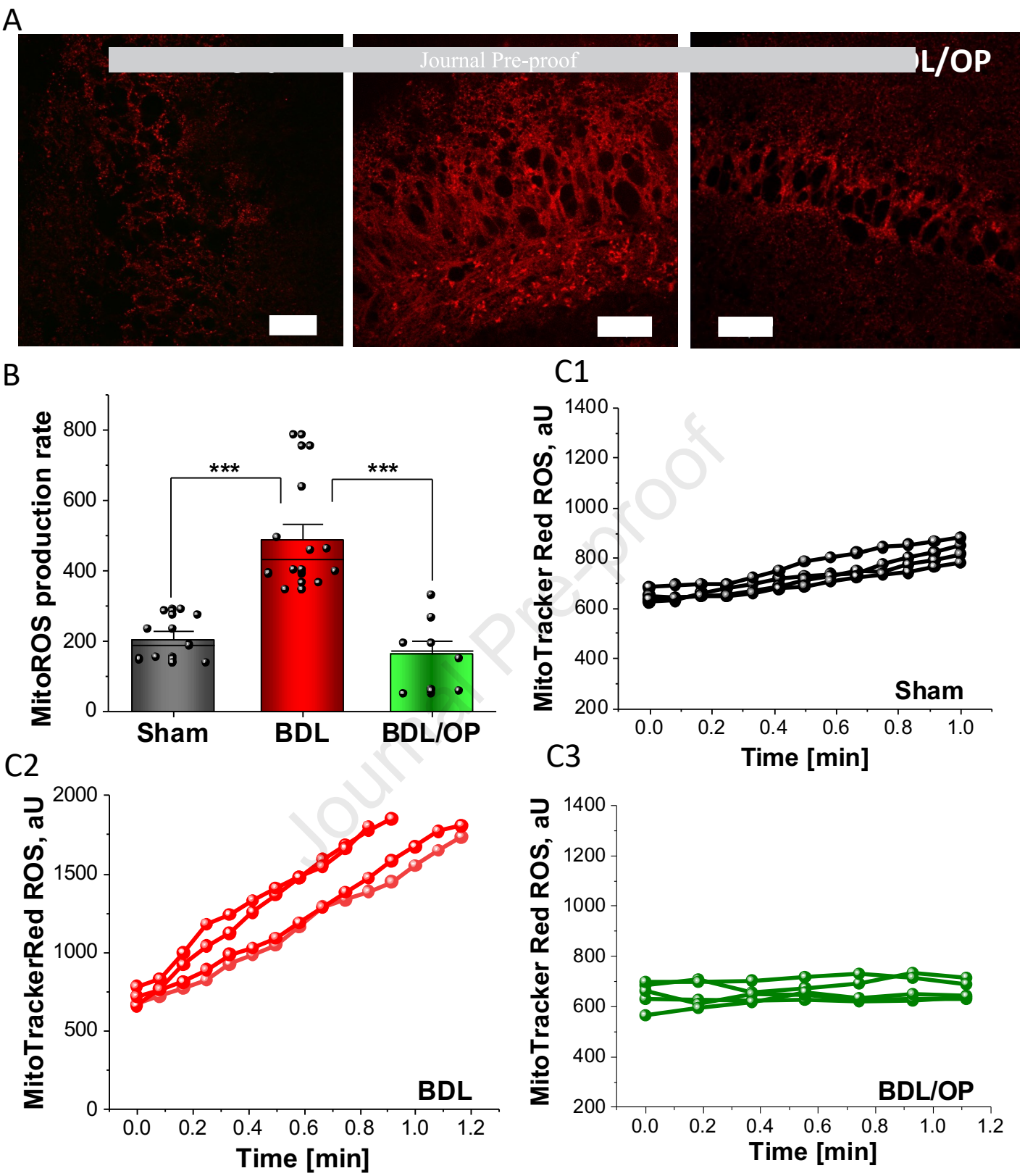

Figure 3.

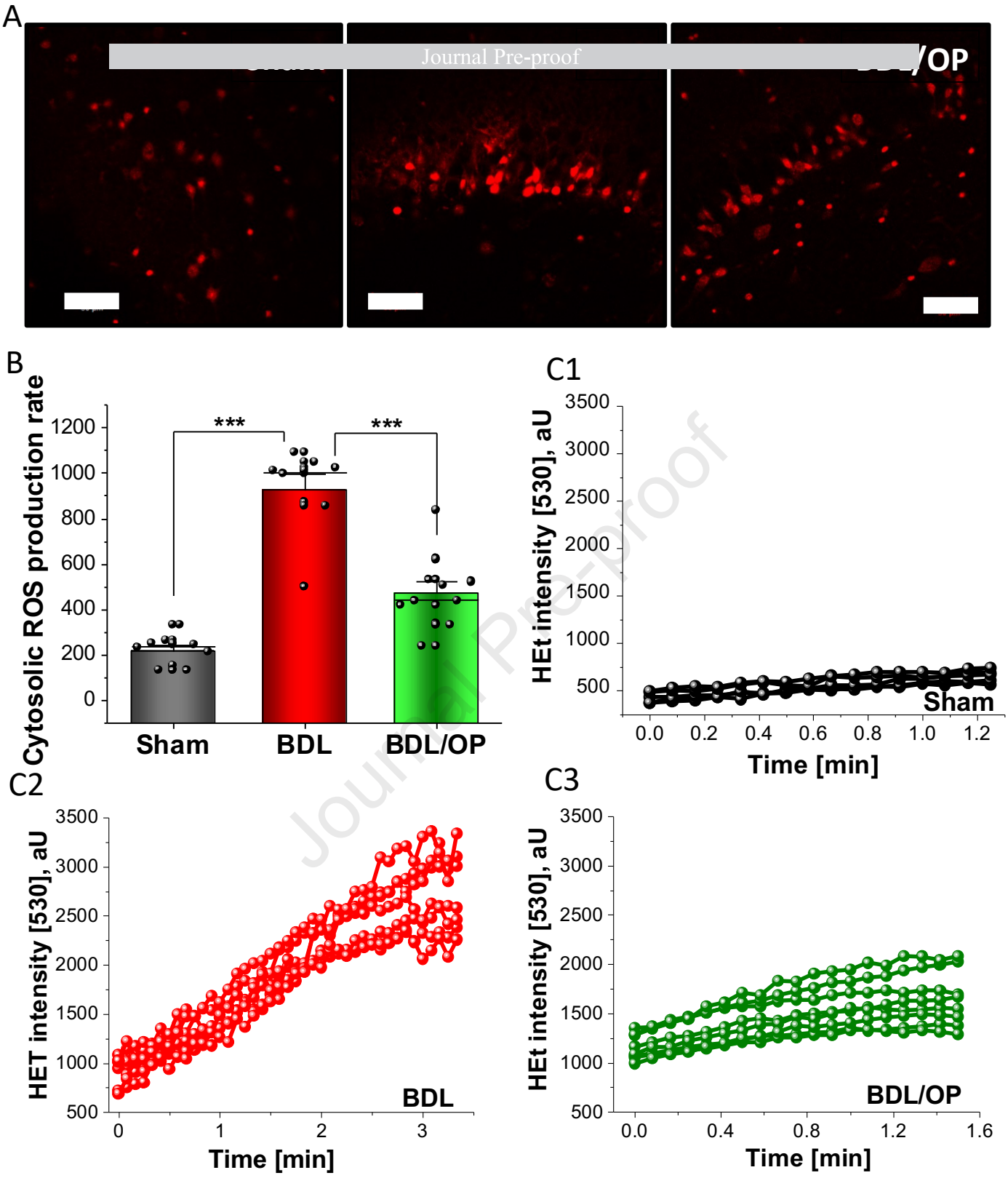

Figure 4.

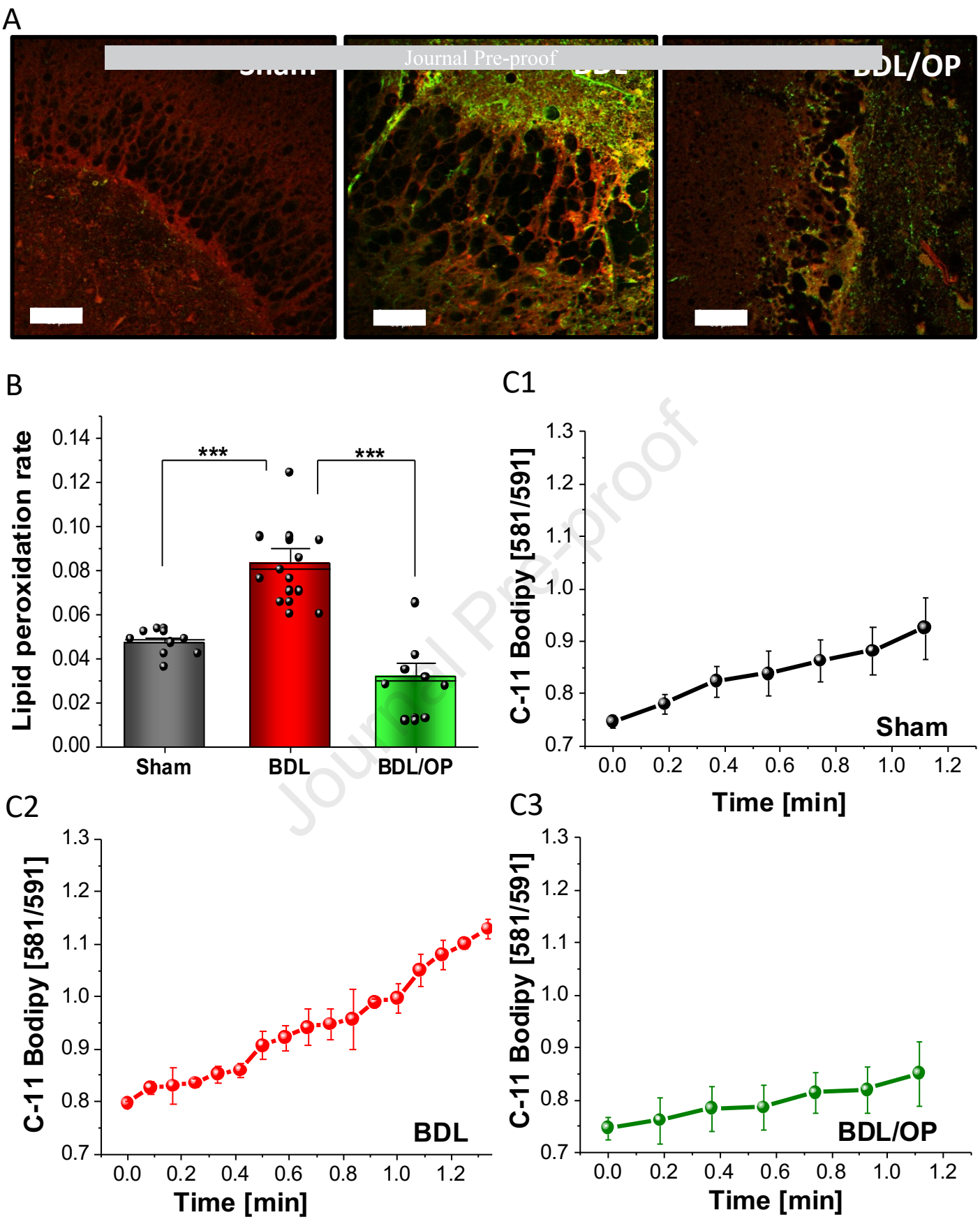

Figure 5.

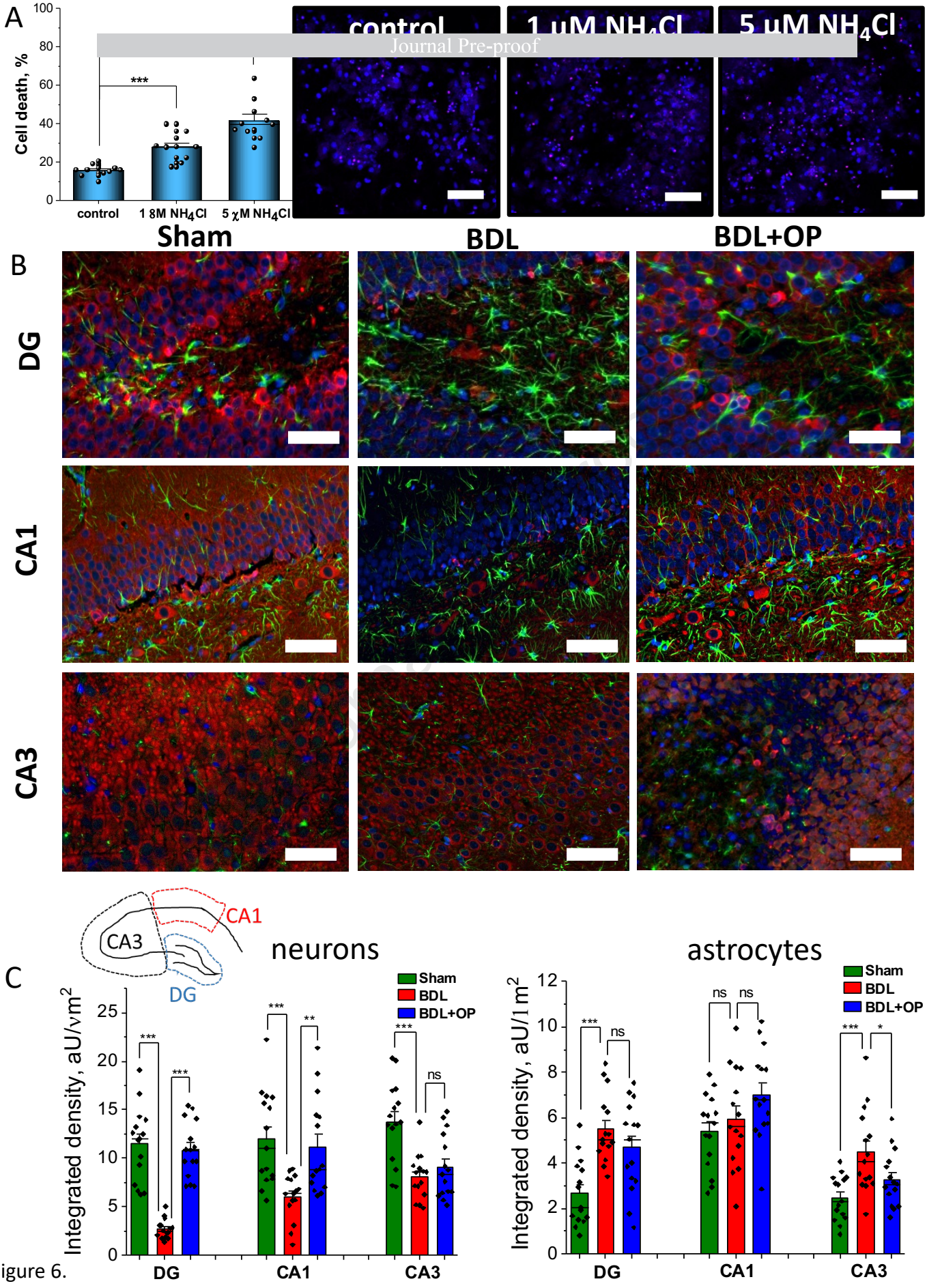

Figure 6.

Highlights

- Low concentrations of ammonia induce mitochondrial dysfunction, overproduction of ROS and cell death in primary neurons.
- Hyperammonemia in cirrhotic rats leads to ROS and LP overproduction, which was prevented by the ammonia scavenger OP.
- In neurons from cirrhotic rats, hyperpolarization of ΔΨm was observed, which was restored by OP treatment.
- In a rat model of liver cirrhosis, profound neuronal loss was observed in the hippocampus.